RSC Advances

Sorption of dyes and Cu(II) ions from wastewater by sonochemically synthesized MnWO4 and MnMoO4 nanostructures

Journal:	*RSC Advances*
Manuscript ID:	RA-ART-07-2014-007618.R1
Article Type:	Paper
Date Submitted by the Author:	12-Aug-2014
Complete List of Authors:	Dutta, Dimple; BARC, Mathur, Aakash; Centre for Converging Nanotechnology, ramkumar, jayshree; barc, Tyagi, A.; BARC, Chemistry

Table of Content

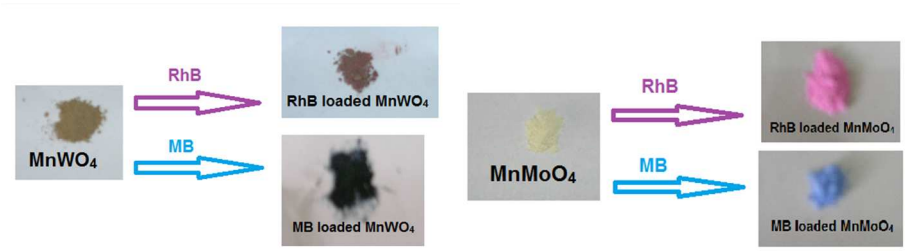

Sonochemically synthesized $MnWO_4$ and $MnMoO_4$ nanomaterials with superior sorption for cationic dyes like Rhodamine B and Methylene Blue.

Sorption of dyes and Cu(II) ions from wastewater by sonochemically synthesized $MnWO_4$ and $MnMoO_4$ nanostructures

Dimple P. Dutta,[a]* Aakash Mathur,[b] Jayshree Ramkumar,[c] Avesh Kumar Tyagi,[a]

[a]Chemistry Division, Bhabha Atomic Research Centre, Mumbai 400 085, India;
[b]Centre for Converging Technologies, University of Rajasthan, Jaipur 302 004, India;
[c]Analytical Chemistry Division, Bhabha Atomic Research Centre, Mumbai 400 085, India.

Tel: +912225592308, Fax: +912225505151, email: dimpled@barc.gov.in

Abstract
$MnWO_4$ and $MnMoO_4$ nanoparticles have been synthesized using a facile sonochemical technique. The nanostructures were characterized by X-ray diffraction (XRD), transmission electron microscopy (TEM) and nitrogen adsorption–desorption measurements. The as-prepared spherical $MnWO_4$ and $MnMoO_4$ nanostructures have a high specific surface area and their excellent adsorbent properties to remove organic pollutants have been demonstrated for the first time. Complete removal of dyes like Rhodamine B and Methylene blue was possible within 2-10 minutes. The influences including initial pH, dosage of adsorbent and contact time have been researched in order to find the optimum adsorption conditions. The experimental data were analyzed by the Langmuir and Freundlich adsorption models. $MnWO_4$ also proved to be a good sorbent for Cu(II) ions. The kinetic modeling for Cu(II) sorption has been discussed. These studies showed that there is a possible application for the complete and fast removal of the organic dyes in presence of inorganic cations using $MnWO_4$/$MnMoO_4$ sorbents. The thermal regeneration of the sorbents is possible and they show similar adsorption efficiency upto ten consecutive cycles. The sonochemically synthesized $MnWO_4$ and $MnMoO_4$ nanomaterials could serve as promising adsorbents for the removal of organic dyes, especially, cationic dye, and Cu(II) ions from polluted water.

Keywords: $MnWO_4$, $MnMoO_4$, adsorption, Rhodamine B, Methylene Blue, Dye Removal

Introduction

Water pollution is considered to be a major environmental issue worldwide. Untreated as well as partially treated effluents from the leather, wool, plastic, cosmetic and paper industries contribute significantly to this pollution load. The textile industries also pose serious environmental problems by releasing large quantities of toxic and carcinogenic dyes in to the water bodies.[1] Apart from degrading the aesthetic beauty of the water bodies, these water soluble dyes also have an inhibitory effect on photosynthesis and pose a serious threat to aquatic life by increasing the chemical oxygen demand (COD) and reducing light penetration and visibility in the water

body.[2,3] Water bodies near metal cleaning and plating facilities, mining, corrosion and electronic device manufacturing units have the added risk of presence of toxic and polluting heavy metals.[4,5] Unfortunately, bio/photodegradation methods are generally not effective for the removal of these dyes and heavy metal ions from the water due to their extreme stability. Hence, alternative methods for wastewater treatment have been an active area of research. Consequently, various physical methods like coagulation and flocculation, oxidation, membrane separation, ultrachemical filtration, chemical treatments, and adsorption have been studied widely for the removal of dyes from aqueous solution.[6-10] Ion exchange and reverse osmosis have showed some promising results in treating diluted metal solutions but at a higher operating cost. Among all these techniques, adsorption based on solid sorbents with large sorption capacity is preferred due to its simplicity, reliability, low consumption of solvent, and the ability to achieve a high level of effectiveness.[11] The thrust area of research is to develop new sorbents which have high adsorptive capacity, are cheap and easily available and can be regenerated using inexpensive processes after their use for sorption. In this regard, much attention has recently been paid to nanomaterials due to its improved sorption characteristics resulting from high surface area.

In the last decade, MWO_4 and $MMoO_4$ (M = Mn, Ca, Zn, Pb, Ba) materials have attracted much attention due to their structural, magnetic and optical properties.[12-16] The most promising mixed metal oxide among these is manganese tungstate ($MnWO_4$) which exhibits high sensitivity to humidity change and has unique magnetic property.[17-20] Consequently, it has attracted considerable research interest for potential applications such as humidity sensors, optical fibers, photoluminescence and scintillator materials.[17,21,22] $MnWO_4$ belongs to the monoclinic $P_{2/c}$ space group, characterized by alternating layers of manganese and tungsten atoms parallel to the (100) plane. Specifically, each Mn and W atom is in an approximately octahedral coordination surrounded by six nearest neighbor oxygen atom sites.[23] Recently, photocatalytic property of $MnWO_4$ and $MnMoO_4$ nanocrystals has also been reported.[24,25] With the advent of nanotechnology it has been demonstrated that larger surface area and remarkable quantum size effect in $MnWO_4$ nano-particles result in lower sintering temperature, faster response to humidity and better photocatalytic activity.[26] However, to the best of our knowledge, there are no reports on the sorption behavior of $MnWO_4$/$MnMoO_4$ nanostructures. Though synthesis of $MnWO_4$ has been reported using conventional solid-state reaction, complexation-precipitation method and sol-gel methods, the particle sizes are in micron scale due to the high temperature

involved either in the synthesis process or during subsequent calcinations.[27,28] Nanostructures of $MnWO_4$/$MnMoO_4$ have been obtained by hydro/solvothermal, combustion and microwave-assisted techniques since they have the advantage of low synthetic temperature.[29-32]

In this manuscript, we report the synthesis of nano-crystalline $MnWO_4$/$MnMoO_4$ by sonochemical method. Sonochemical synthesis is based on acoustic cavitation resulting from the continuous formation, growth and implosive collapse of the bubbles in a liquid.[33,34] The synthesis has been carried out in the absence of any capping agent and it is also a surfactant free and template free technique which ensures easy recovery of the final product. The nanoparticles so obtained were characterized using powder XRD and TEM. For the sorption studies, common dyes like rhodamine B and methylene blue were selected. The sorption affinity of these $MnWO_4$/$MnMoO_4$ nanostructures for heavy metal ions such as copper was also tested. This is due to the fact that though copper is an essential nutrient in trace amount, at higher level it is toxic to plants, algae and humans. Excess copper tends to accumulate in the liver, can cause stomach cancer and can be toxic to fish at lower pH values.[35] The sonochemically synthesized as-prepared $MnWO_4$/$MnMoO_4$ nanostructures are expected to be new promising materials for industrial dye as well as copper effluent remediation. The details of this work are discussed herein.

Experimental Section

All the reactions were carried out under ambient conditions. High purity (≥ 99%) AR grade manganese nitrate [$Mn(NO_3)_2.xH_2O$], sodium tungstate [$Na_2WO_4.2H_2O$] and sodium molybdate [$Na_2MoO_4.2H_2O$] were obtained from commercial sources.

Synthesis of $MnWO_4$

In a typical reaction, an aqueous solution [$Na_2WO_4.2H_2O$] (11.39 g, 34.52 mmol) was added dropwise to an aqueous solution of [$Mn(NO_3)_2.xH_2O$] (6.17 g, 34.52 mmol). The system was then irradiated with high intensity (100 W/cm^2) ultrasonic radiation (Oscar Ultrasonics) operating at 40 kHz, under air for 1.5h. The titanium horn was inserted to a depth of 6 cm in the solution. The reaction cell was not thermostated and the final temperature was 55 °C. After sonication, the precipitate was washed with deionized water and centrifuged at 5000rpm for 2min. The ochre precipitate obtained was dried in air.

Synthesis of $MnMoO_4$

An aqueous solution [$Na_2MoO_4.2H_2O$] (4.86 g, 20.1 mmol) was added dropwise to an aqueous solution of [$Mn(NO_3)_2.xH_2O$] (3.60 g, 20.1 mmol). The system was then irradiated with high intensity (100 W/cm^2) ultrasonic radiation (Oscar Ultrasonics) operating at 40 kHz, under air for 1h. The titanium horn was inserted to a depth of 6 cm in the solution. The reaction cell was not thermostated and the final temperature was 40 °C. After sonication, the precipitate was washed with deionized water and centrifuged at 5000rpm for 2min. The off-white precipitate obtained was dried in air.

Calcination of $MnWO_4$ and $MnMoO_4$

A portion of the as prepared samples were calcined in furnace at 500°C for 3h.

Materials Characterization

X-Ray diffraction (XRD) measurements were carried out on a Philips Instrument, operating with monochromatized Cu-Kα radiation (λ = 1.5406 Å) and employing a scan rate of 0.02 °/ s in the scattering angular range (2θ) of 10° to 80°. Silicon was used as an external standard for correction due to instrumental line broadening. The average crystallite size was calculated from the diffraction line width based on Scherrer's relation: $d = 0.9\lambda/\beta\cos\theta$, where λ denotes the wavelength of X-rays and β is the corrected full width at half maxima (FWHM). Conventional TEM micrographs were recorded on Carl Zeiss instrument operating at 120kV. The particulates so obtained, were dispersed in methanol solution and then deposited on the carbon coated copper grids for TEM studies. The specific surface area of manganese tungstate/molybdate nanoparticles was determined using a Bel Japan Inc., Belsorp II surface area analyzer by measuring N_2 adsorption and adopting the well-known BET procedure. The Infrared spectra were taken in the JASCO FTIR (V-610) spectrophotometer with KBr pellets.

Sorption Studies

Dye removal experiments

The sorption studies of each of the individual dyes viz. rhodamine B (RhB) and methylene blue (MB) were carried out in the batch mode. The batch mode experiments involved equilibration of a known concentration of the dye maintained at a particular pH for a known period of time with

accurately weighed amount of the sorbent at room temperature. The pH values of the solutions were adjusted according to need by using HCl or ammonia solution. Once the equilibration was complete, the amount of dye left behind in solution was measured spectrophotometrically (Shimadzu, UV-1650) by observing the absorbance at 546 and 617 nm for RhB and MB, respectively. The various experimental conditions of pH, amount of sorbent, equilibration time and initial dye concentration were varied to get a complete understanding of the sorption process. The data in these studies were obtained from average of triplicate measurements.

Regeneration of the $MnWO_4$ and $MnMoO_4$ sorbents

After the completion of the adsorption process, the $MnWO_4$/$MnMoO_4$ sorbent was extracted from solution by centrifugation and washed with deionized water repeatedly. Then, after drying in a freeze dryer, the powders of the RhB/MB adsorbed sorbents were annealed at 225°C for 0.5 h under air.

Copper removal experiments

The uptake studies were carried at room temperature (25°C) in batch mode using aqueous solutions containing copper ion. Ten milliliters of aqueous copper ion solution of known concentration at a particular pH was equilibrated with a weighed amount of $MnWO_4$/$MnMoO_4$ sample for a known period of time. The concentration of metal ion left behind in solution after equilibration was determined. The pH of the solution before and after equilibration was also measured. The solution after equilibration was analyzed completely for the presence of copper ions by complexation with PAR ligand using UV-visible spectroscopy and measuring the absorption at 545nm. The samples after equilibration were again characterized using XRD technique.

Results and Discussion

The XRD pattern of the as prepared $MnWO_4$ sample is shown in Figure 1a, which reveals the crystalline nature of the product. The XRD patterns are consistent with standard data for monoclinic crystal system of $MnWO_4$ with P2/c space-group symmetry (JCPDS file no. 72-0478). The calculated lattice parameters of a = 4.821Å, b = 5.74Å, c = 4.99Å are very close to that of the reported values. The average crystallite size calculated using the Debye-Scherrer

equation from the FWHM (full width half maxima) of XRD peaks was found to be ~12 nm. On calcining the as synthesized product at 500°C for 3h, a vast improvement in the crystallinity was observed as is evident from the XRD pattern which shows an increase in the peak intensity and sharpness (Figure 1b). However, there is no change in diffraction positions indicating that the monoclinic phase is quite stable. Application of the Debye-Scherrer equation to the FWHM of XRD peaks yields an average crystallite size of ~35 nm.

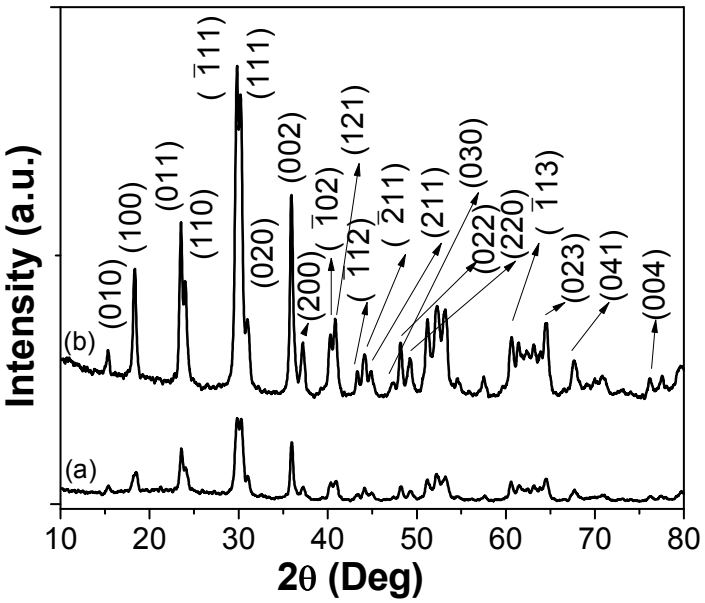

Figure 1: Powder XRD of (a) as prepared and (b) thermally treated $MnWO_4$

Figure 2a shows the diffraction data obtained for the as prepared $MnMoO_4$ sample. All the diffraction peaks can be indexed to monoclinic α-$MnMoO_4$ according to the JCPDS card no. 822166. The space group is C2/m and the lattice parameters of a = 10.45Å, b = 9.53Å and c = 7.14Å match well with those of the reported compound. In monoclinic structure, the Mn atoms are octahedrally coordinated with oxygen while Mo atoms are tetrahedrally coordinated with oxygen in C2/m space group arrangement.[36] The average crystallite size calculated using the Debye-Scherrer equation from the FWHM of XRD peaks was found to be ~25 nm. On heating the as prepared product at 500°C for 3h, there was no change in the XRD pattern which indicates the stability of the monoclinic phase (Figure 2b). A slight increase in the average crystal size of the sample to ~30nm was observed after heating.

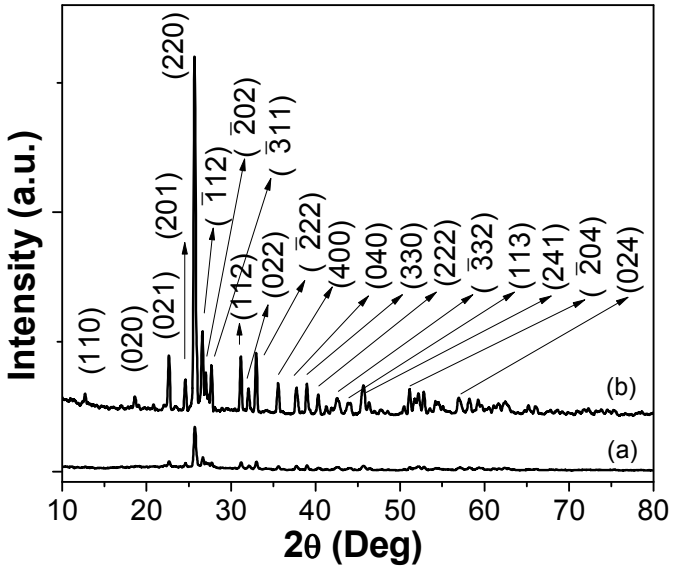

Figure 2: Powder XRD of (a) as prepared and (b) thermally treated $MnMoO_4$

To further investigate the microstructure and topography, we used transmission electron microscopy to image the $MnWO_4$ and $MnMoO_4$ samples on carbon coated copper TEM grids. The TEM image of the as prepared $MnWO_4$ shows formation of relatively monodispersed spherical particles with diameter of ~12-15 nm (Figure 3a). The morphology of the heated $MnWO_4$ sample was also studied using TEM. It can be observed in Figure 3b that on heating, the size of the $MnWO_4$ particles increased to ~30-35 nm but their spherical shape has been retained. In case of $MnMoO_4$, the particles were somewhat aggregated and have a spherical or very close to spherical morphology (Figure 3c). The particle size distribution ranged between 25 to 30 nm. There was not much change in the size and morphology of the $MnMoO_4$ particles on heating as is evident from Figure 3d. The sizes of the nanoparticles obtained from TEM images are consistent with the calculated values obtained from the XRD data.

The specific surface area of the $MnWO_4$/ $MnMoO_4$ nanoparticles was measured using the BET procedure. It is determined by physical adsorption of a gas on the surface of the solid and by measuring the amount of adsorbed gas corresponding to a monomolecular layer on the surface.[37] From the BET analysis, we found that the as prepared $MnWO_4$ nanoparticles have an average specific surface area of 127.0 ± 0.4 m^2/g whereas in case of the heated sample it reduces to 42 ± 0.2 m^2/g. This can be explained since heating results in the formation of larger sized $MnWO_4$

nanoparticles leading to less specific surface area. The average specific surface area of the as prepared $MnMoO_4$ nanoparticles was found to be 112 ± 0.5 m^2/g. On calcination, the average surface area marginally reduces to 98 ± 0.2 m^2/g which is acceptable since the TEM micrographs clearly showed that there was negligible change in size of the nanoparticles on heating.

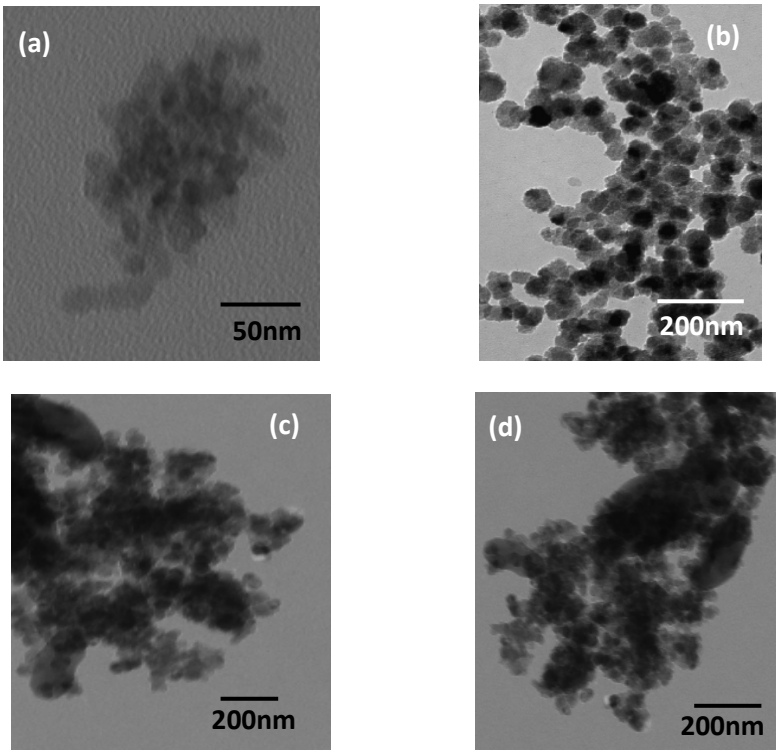

Figure 3: TEM image of (a) as prepared $MnWO_4$, (b) thermally treated $MnWO_4$, (c) as prepared $MnMoO_4$ and (d) thermally treated $MnMoO_4$.

The sorption studies carried out in the batch mode gave an idea of the sorption behavior of nano manganese tungstate/molybdate with respect to different organic and inorganic toxic species. The sorption efficiency of these nanomaterials was evaluated for the uptake of dyes like Rhodamine B (RhB) and methylene blue (MB) and inorganic Cu(II) ions. The solution pH, concentration of $MnWO_4$/$MnMoO_4$ nanoparticles, and initial dye concentration were the variables in this study. Since Rhodamine B is a cationic dye, it is expected that the pH of the dye solution can affect the sorption process. In order to study this effect, a known amount of the sorbent was equilibrated with the RhB dye solutions of known concentration (20ppm) maintained at varying pHs (1-9) for different equilibration periods. It is seen that the kinetics of

sorption depends on the pH of the external solution. The optimum pH for effective and fast sorption was 3 and hence all the further sorption studies were carried out at this pH. The pH dependence of the sorption gives an idea that the process follows an ion exchange mechanism.

The time of equilibration is one of an important parameter which determines the kinetics of the reaction. Figure 4a shows a typical curve in which the change in the absorbance of 20 ppm RhB dye solution was monitored over a period of time on 10mg unheated $MnWO_4$ nanoparticles. It is seen that the kinetics of the reaction is very fast and the sorption is completed within 10 min. The amount of nanotungstate added was optimized after doing several experiments where different amounts of $MnWO_4$ were added to 20ppm of dye. The results indicated that 10mg was the optimum amount which leads to complete adsorption of the dye within 10 minute. Less than this amount resulted in slightly longer time for complete removal of the dye. The effect of initial concentration of the dye on the sorption process was studied by varying the dye concentrations from 10 to 50 mg/L in solution maintained at pH 3 and equilibrated for 10 minutes. It was observed that the time needed for complete removal of RhB was around 10 minutes for the concentration range of 10-50 mg/L. The heated $MnWO_4$ samples on the contrary did not exhibit much sorption characteristics even after 16h of equilibration (Figure 4b). This proves that this superior adsorbent property manifested by the sonochemically synthesized as prepared $MnWO_4$ samples, is primarily due to its morphology and high surface area in the nano dimensions.

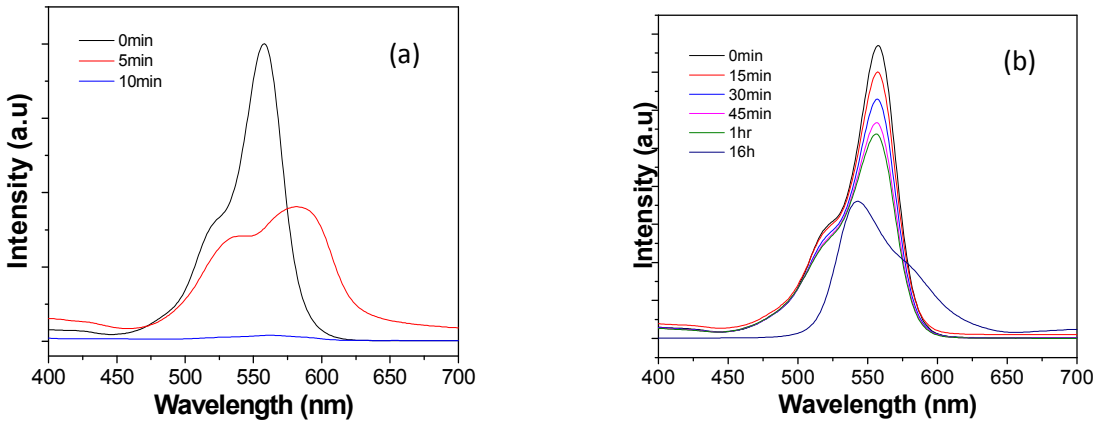

Figure 4: Change in the absorbance of RhB dye solution monitored over a period of time for (a) as prepared $MnWO_4$ and (b) thermally treated $MnWO_4$.

The same series of sorption experiments were also carried out with Methylene blue (MB). It was seen that at pH 2, the complete removal of MB was achieved within 10 mins whereas the complete removal was within 2 mins at pH 3. The variation of pH studies showed that the optimum pH for MB removal in case of $MnWO_4$ was pH ~ 3-5 and further studies were carried out at pH of 3. The removal of Cu(II) ions was also carried out in this pH range for comparison. In case of the as prepared $MnMoO_4$, the kinetics of the reaction is very fast and the sorption of RhB as well as MB is completed within 2 min under acidic pH. At neutral and basic pH there is no adsorption even after 20 min which indicates that the process follows an ion exchange mechanism. The comparative effect of pH on the sorption efficiency of $MnWO_4$ and $MnMoO_4$ nanosorbents for both RhB and MB is shown in Figure 5.

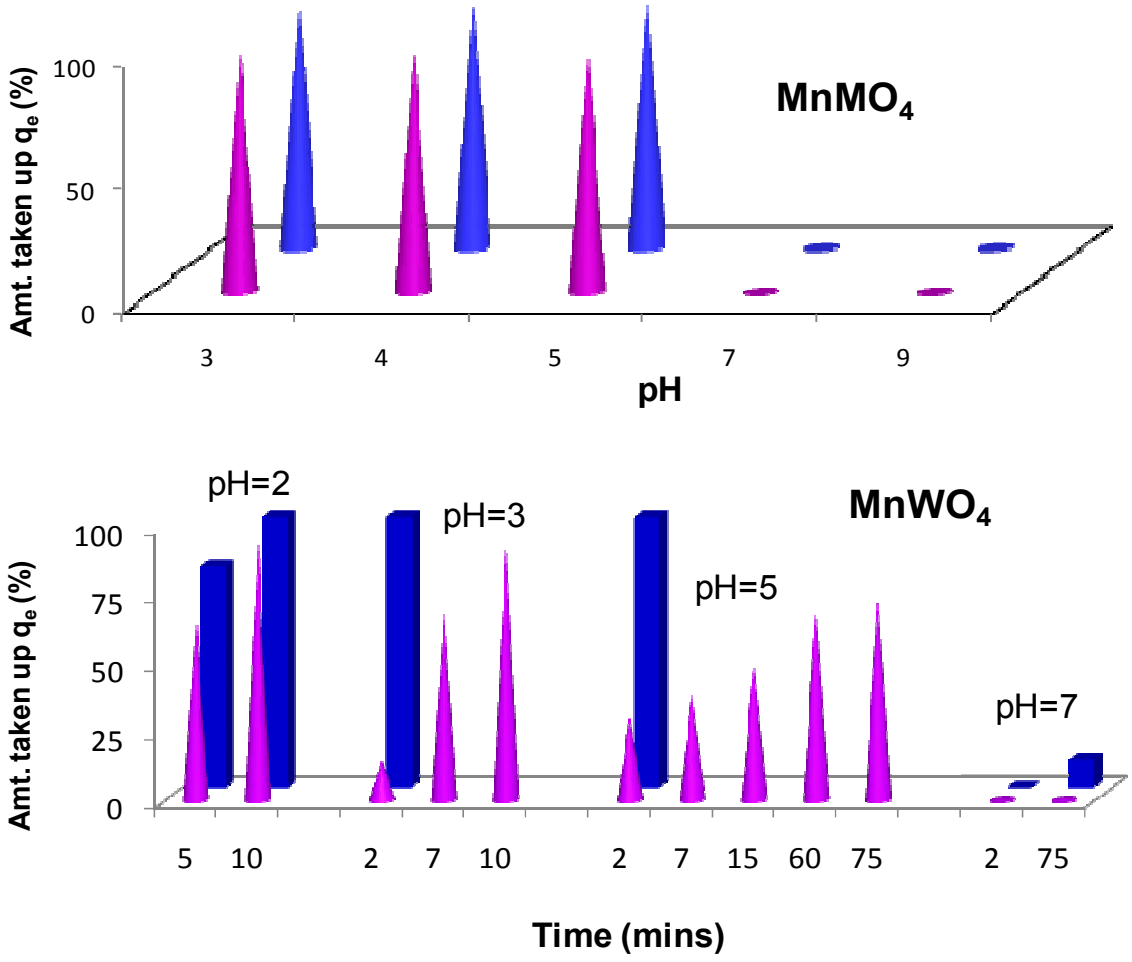

Figure 5: Effect of pH on the sorption efficiency of $MnMoO_4$ and $MnWO_4$ nanosorbents (10mg) for 20ppm RhB (pink) and 20ppm MB (blue) dyes.

The time needed for complete removal of the RhB dye was around 2 minutes for the concentration range of 20-200 mg/L. However, in the same period, the sorption efficiency for a 200 mg/L concentration of MB was around 85% and it required about 5 minutes for complete sorption. It is to be noted that the adsorption rate of our sonochemically synthesized as prepared $MnWO_4$/$MnMoO_4$ for the dyes is much faster than that reported for other nanosorbents like Fe_3O_4@C, magnetite, activated carbon, MnO_2, fly ash, red mud, MCM 22, etc.[38-45] In all these cases, the time taken for MB adsorption ranges to a few hours whereas for our sonochemically synthesized as prepared $MnWO_4$/$MnMoO_4$, ~100% sorption is completed in a few minutes. Table 1 gives the comparative effect of time of equilibration on the sorption efficiency of 10mg $MnWO_4$ /$MnMoO_4$ nanosorbents for 100ppm of Cu(II) ions and RhB and MB dyes. It can be seen that the removal of the dyes occurred very fast as compared to the Cu(II) ions. With as prepared $MnMoO_4$ sorbent, the removal of both the dyes was achieved within 2 min whereas the copper ion removal was possible in 300 minutes. For the sorption with as prepared $MnWO_4$, it was seen that MB was removed within 2 min whereas both RhB and Cu (II) needed 10 mins and 15 mins respectively for complete removal. Therefore it was observed that the nature of the sorbent had a key role in the kinetics of sorption.

Table 1: Effect of time of equilibration on the sorption efficiency of 10mg of $MnMoO_4$ /$MnWO_4$ nanosorbents for 100ppm of Cu(II) ions and RhB and MB dyes.

Sorbent (10mg)	**Time taken for maximum uptake (min)**		
	RhB	**MB**	**Cu(II)**
As prepared $MnWO_4$	**10**	**2**	**15**
As prepared $MnMoO_4$	**2**	**2**	**300**

From Figure 6 it is seen that for both the sorbents the uptake of the dyes is nearly complete whereas the sorption of Cu(II) ions is around 75 and 89.8 % for $MnWO_4$ and $MnMoO_4$, respectively. Thus these present studies showed that there is a possible application of these sorbents for the complete and fast removal of the organic dyes in presence of inorganic cations.

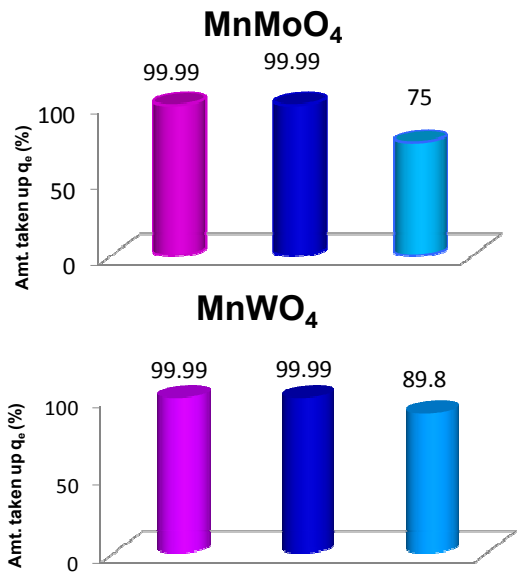

Figure 6: Effect of nature of the adsorbent (100ppm each) on the sorption capacity of as prepared $MnMoO_4$ and $MnWO_4$ sorbents.

The amount of dye/Cu(II) adsorbed onto unit weight of adsorbent at equilibrium, q_e (mg/g) was calculated using the mass balance equation given by:

$$q_e = \frac{(C_0 - C_e)V}{m} \qquad (1)$$

where m is mass of sorbent (g), V is the volume of the solution (L), C_0 represent the initial concentration of dye/Cu(II) (mg/L) and C_e is the instant concentration of the dye at predetermined time t. The effect of initial concentration of the dye/Cu(II) on the sorption of $MnWO_4$ was studied by varying the concentration in the range of 20-100 ppm for each of them and the results are shown in Figure 7. It is seen that in the present study, the uptake capacity has not reached the maximum and this is an indication that the sorbents can be used for the uptake of dye/Cu(II) at concentrations higher than 100 ppm.

In contrast to $MnWO_4$, the $MnMoO_4$ nanoparticles showed no change in their adsorption properties even after heating at 500°C for 3h. This shows that adsorption in this case is not merely dependent on the morphology and high surface area of the $MnMoO_4$ nanoparticles but also on the inherent nature of the sorbent.

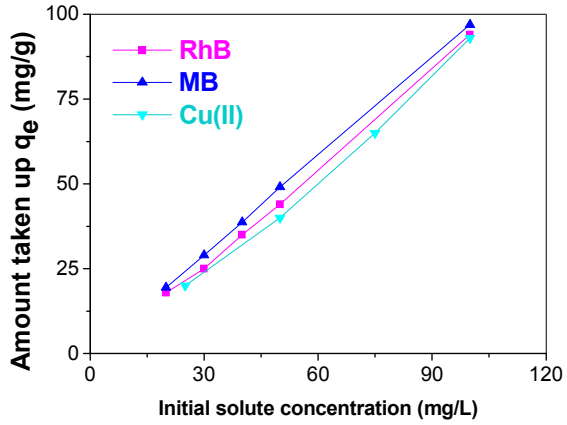

Figure 7: Effect of initial concentration of RhB, MB and Cu(II) ions on the amount taken up by as prepared $MnWO_4$ nanosorbent

The sorption data were fitted to both equilibrium and kinetic modeling to get an overall idea of the sorption process. Equilibrium modeling was carried out using the most fundamental models of Langmuir and Freundlich using the linearised equations for these isotherms. The main consideration of the Langmuir isotherm is sorption that occurs at specific homogeneous sites within the adsorbent, indicating a monolayer adsorption process (constant heat of adsorption for all sites). The Freundlich adsorption isotherm, which is generally based on multilayer adsorption on heterogeneous surface, holds the assumption that the adsorption sites are distributed exponentially with respect to the heat of adsorption. The results of these modelling are given in Figure 8. It is seen that the experimental sorption data fits the Freundlich rather than the Langmuir model as seen from the R^2 values (0.9998 and 0.9734, respectively) of the fitted curves. The maximum sorption capacity evaluated is 250, 230 and 200 mg/g respectively for MB, RhB and Cu(II) with as prepared $MnWO_4$. In case of as prepared $MnMoO_4$, the sorption capacities calculated for MB, RhB and Cu(II) are 225, 210 and 175 mg/g respectively. The reason for the high uptake capacity can be attributed to the fact that sorption is probably not restricted only to monolayer. The fact that Freundlich model is applicable indicates that probably the sorption energy for each molecule may be different due to the variations in the surface property of the nanostructures. The maximum sorption capacity of MB in case of our samples is higher than that reported for traditional sorbents like silica gel (~195mg/g) but less than that reported for activated clay mineral (~350mg/g).[46,47] However, in case of activated clay, the time taken for complete sorption is 2h whereas in our case the sorption is complete in a few minutes.

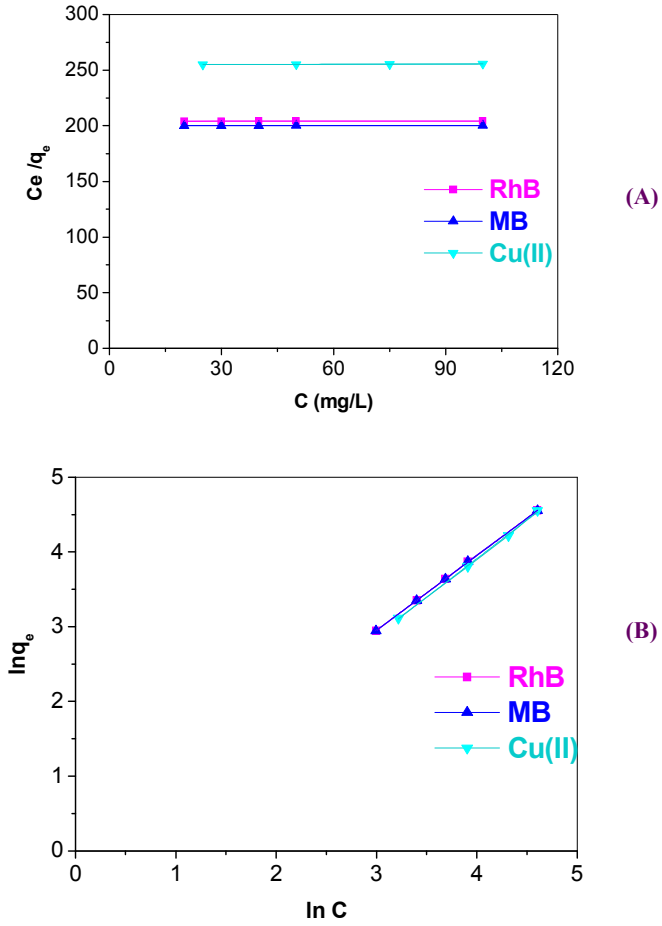

Figure 8: Equilibrium modeling of the sorption processes using (A) Langmuir Isotherm and (B) Freundlich Isotherm for as prepared $MnWO_4$ nanosorbent.

The kinetic modeling was not carried out for the sorption using nano $MnMoO_4$ as the kinetics is so fast that it was not possible to measure various points within the small time periods. However, the kinetics for Cu(II) sorption was carried out. Figure 9 shows the effect of time of equilibration on the sorption of Cu(II) by the as prepared $MnWO_4$/$MnMoO_4$ nanosorbents. It is seen that $MnWO_4$ shows higher uptake than $MnMoO_4$.

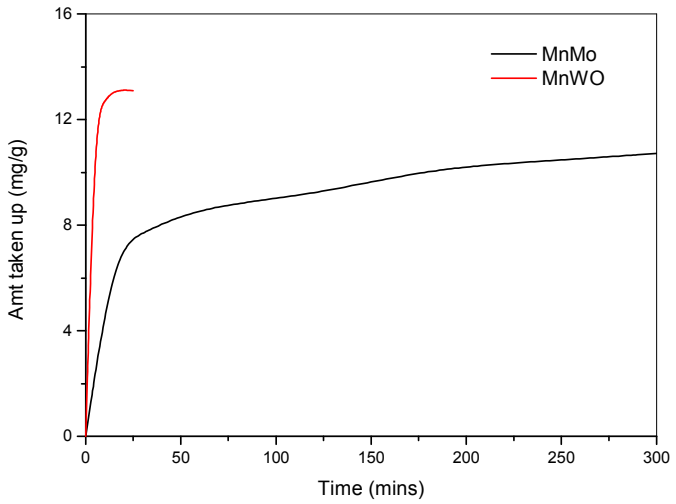

Figure 9: Effect of time of equilibration on the sorption of Cu(II) by as prepared $MnMoO_4$ and $MnWO_4$.

In order to distinguish the kinetics equation based on the adsorption capacity of solid from the concentration of solution, Lagergren's first-order rate equation has been called pseudo-first-order since 1998.[48] A second-order kinetic expression for the adsorption was reported by Ho.[49] In order to distinguish the kinetic equation based on the adsorption capacity of solid from the one that is based on the concentration of solution, Ho's second-order rate expression has been called pseudo-second order. The linearised equations for the pseudo-first-order and second-order models are given by equation 2 and 3. In these equations q_e and q_t are the amount of solute on the surface of the sorbent (mmol/g) at equilibrium and at time t respectively.

$$\log(q_e - q_t) = \log q_e - \frac{K_{ads} * t}{2.303} \quad \text{..... (2)}$$

$$\frac{t}{q_t} = \frac{1}{K_{2ads} q_e^2} + \frac{t}{q_e} \quad \text{..... (3)}$$

The slope of the straight line plots of log ($q_e - q_t$) against t will give the values of the first order rate constant K_{ads} whereas from the plot of t/q_t versus time t, the value of K_{2ads} can be calculated. The results of the kinetic modeling are given in Figure10 and it appears that both the models are applicable. However a closer look at the R^2 values of the linear fits, it is seen that the pseudo first order model with a better R^2 value of 0.9996 as compared to 0.8388 for pseudo second order model is more applicable. The first order rate constant for the Cu(II) sorption on nanomolybdate and tungstate are calculated to be 0.001 and 0.003 min^{-1} respectively.

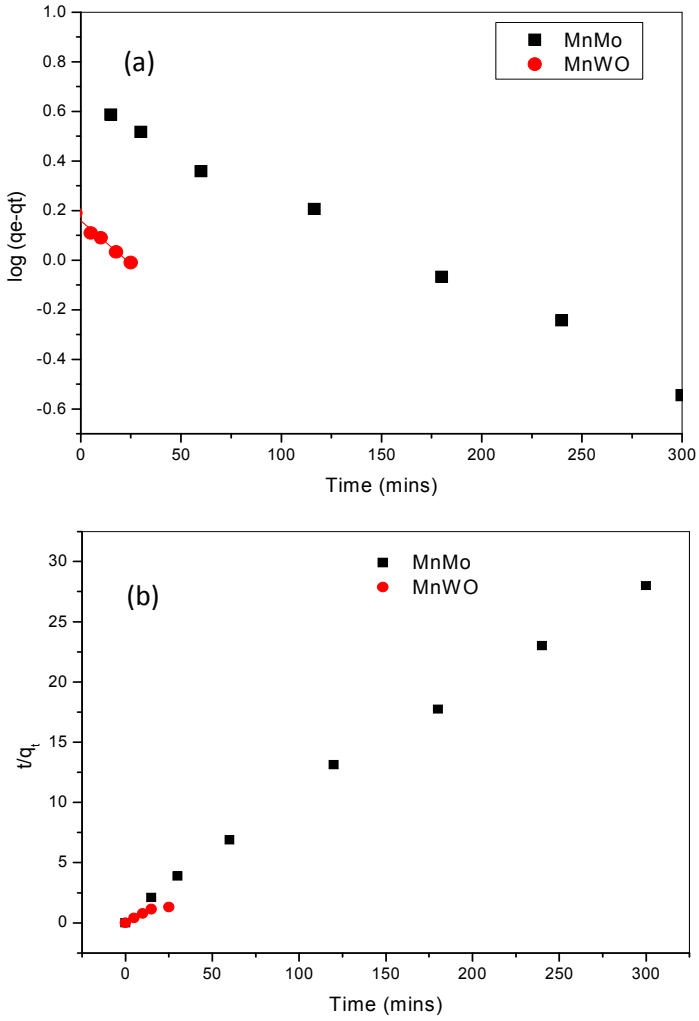

Figure10: Kinetic modelling of Cu(II) sorption by as prepared $MnWO_4$ and $MnMoO_4$ nanosorbents using (a) first order model and (b) second order model.

Our sonochemically synthesized $MnWO_4$ crystallizes in the monoclinic P2/c space group with two formula units per primitive cell. The distribution of the optical modes among the irreducible representations of the factor group C_{2h} is $8A_g + 7A_u + 10B_g + 8B_u$. This can be further subdivided into $2A_g + A_u + 4B_g + 2B_u$ lattice translational modes of the Mn^{2+} and W^{6+} ions, and $6A_g + 6A_u + 6B_g + 6B_u$ internal modes involving oxygen atoms. Internal modes can be subdivided into $3A_g + 3B_g$ symmetric stretching (ν_s(W–O–W)) and symmetric bending (δ_s(W–O–W)) vibrations of the double WOOW oxygen bridge, $3A_u + 3B_u$ antisymmetric stretching

(ν_{as}(W–O–W)) and antisymmetric bending (δ_{as}(W–O–W)) vibrations of the double WOOW oxygen bridge modes, $A_g + A_u$ ($B_g + B_u$) symmetric (antisymmetric) stretching of the WO_2 groups ($\nu_s(WO_2)$ and $\nu_{as}(WO_2)$), $A_g + A_u$ scissoring ($\delta_{sc}(WO_2)$), $B_g + B_u$ rocking ($\rho(WO_2)$), $A_g + A_u$ twisting ($\tau(WO_2)$) and $B_g + B_u$ wagging modes ($\omega(WO_2)$). According to the selection rules, all g modes ($8A_g + 10B_g$) are Raman active and all u modes ($7A_u + 8B_u$) are IR active. The IR spectrum of nano $MnWO_4$ (Figure 11a) shows a number of absorption bands (located at 418, 493, 583, 673 and 860 cm^{-1}) in the range of 500–1000 cm^{-1} which are similar to that of the bulk IR pattern previously reported for $MnWO_4.H_2O$, wherein the inorganic modes lie at the low-wavenumber end of the spectra.[50] Many of these infrared bands can be assigned to internal stretching modes, i.e. $\nu_3(A_u)$ and $\nu_3(E_u)$ transitions.[51] In case of RhB loaded as prepared $MnWO_4$, reductions in the peaks at 493, 583, 673 and 860 cm^{-1} were seen, but the peak positions did not change. This clearly indicates the adsorption of dye on the as prepared $MnWO_4$ surface by physisorption instead of chemical combination.

The IR spectrum of nano $MnMoO_4$ (Figure 11b) shows a number of absorption bands (located at 750, 798, 830, 870, 905 and 941 cm^{-1}) in the range of 500–1000 cm^{-1}. The observed four absorption bands 941, 912, 870 and 798 cm^{-1} clearly reveal that α-$MnMoO_4$ has Mo in tetrahedral coordination with oxygen. The band at 941 cm^{-1} could be assigned to the Mo=O group.[52] The absorption bands at 941 cm^{-1} indicate symmetric MoO_4 stretching while those near 870 and 798 cm^{-1} indicate asymmetric MnO_6 stretching.[52] The broad absorption band at 750 cm^{-1} is associated with the Mo–O stretching vibration.[53] Hence, from the FT-IR spectra the formation of single phase α-$MnMoO_4$ can be evidenced. In case of RhB loaded as prepared $MnMoO_4$, change in peak positions was observed and a new broad peak at ~590cm^{-1} appeared. This shift in peak values may be due to the formation of chemical bond between functional groups present on $BaMoO_4$ and RhB. This indicates the adsorption of dye on the $MnMoO_4$ surface is by the process of chemisorption. It is probably this process of chemisorption of the dyes on the surface of nano $MnMoO_4$ which leads to its better sorption efficiency compared to nano $MnWO_4$.

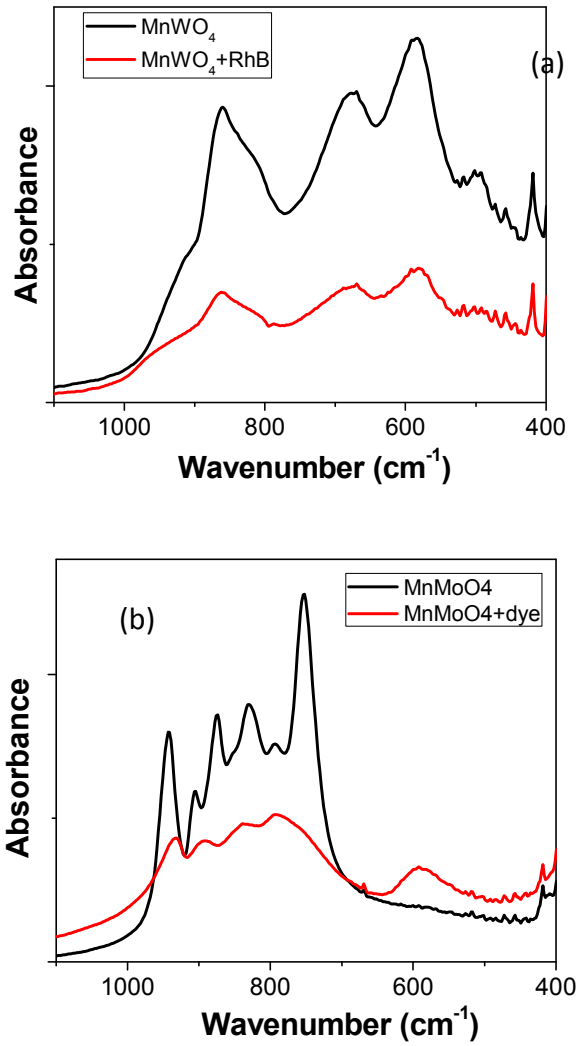

Figure 11: FTIR spectra of as prepared and dye adsorbed (a) $MnWO_4$ and (b) $MnMoO_4$ nanoparticles.

Figure 12 shows the DRS profile of the adsorbed RhB dye (20ppm) on the nano $MnMoO_4$ surface. The DRS profile of the RhB dye is also shown for ready comparison. We find that upon adsorption there is a change in the peak of the absorption profile of the dye. The RhB dye has a broad band with a maximum absorption centered at λ_{max} = 520 nm with a small shoulder at 594nm. However for the adsorbed RhB on $MnMoO_4$ this peak shifts to a higher value of 562nm and the shoulder peak vanishes. Also the FWHM of this 562 nm peak is less than that observed for the pure RhB dye. The peak shift to higher entity and the decrease in the FWHM value shows that there is definitely some electronic interaction between the $MnMoO_4$ surface and the RhB dye. Therefore this process of adsorption of the RhB on $MnMoO_4$ is a process of chemisorption

(mild electronic interaction) rather than that of physisorption, however not to the extent of reactive chemisorption. This dye loaded as prepared $MnMoO_4$ sample was heated at 225°C in a furnace to check the possibility of thermal regeneration of the adsorbent. The diffuse reflectance UV-vis spectra of the original as well as furnace heated dye loaded $MnMoO_4$ were similar which proves that upon thermal treatment there is a complete removal of the dye from the surface and also there is no decomposition of the dye on this surface. This type of thermal regeneration of the adsorbent at moderate temperature is unlikely in case of reactive chemisorption. For practical application of a sorbent, it needs to be stable. We have tested the sorption capacity of the regenerated $MnMoO_4$ sample upto ten consecutive cycles and did not observe any noticeable difference in its performance which indicates the stability of the $MnMoO_4$ sorbent. The crystalline structure of the thermally regenerated $MnMoO_4$ after ten consecutive RhB adsorption cycles was also monitored. The corresponding powder XRD pattern for the sorbent recovered after ten runs matches exactly with the starting sample which indicates its high stability (Figure 13).

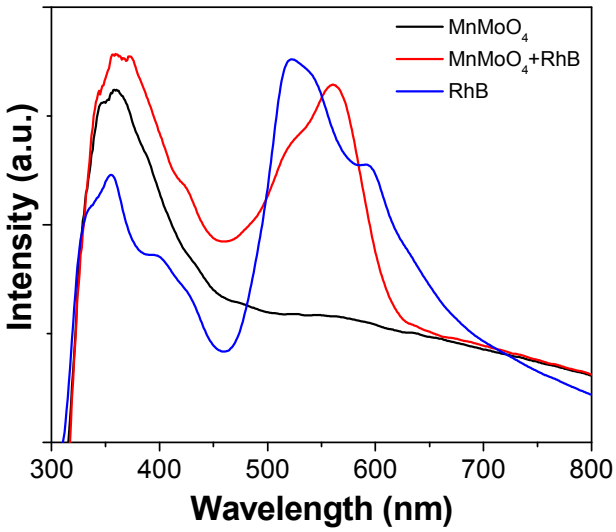

Figure 12: Diffuse reflectance UV-vis spectra of the adsorbed RhB dye on the as prepared $MnMoO_4$ surface.

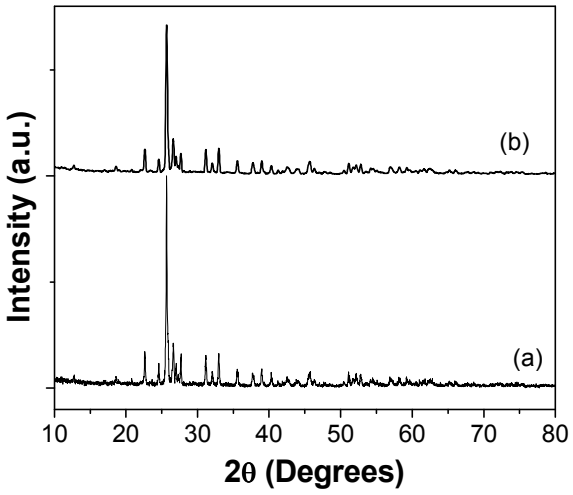

Figure 13: Powder XRD pattern of (a) as prepared $MnMoO_4$ and (b) thermally regenerated $MnMoO_4$ after ten adsorption cycles.

Conclusion

A facile sonochemical technique for the synthesis of spherical $MnWO_4$ and $MnMoO_4$ nanoparticles has been developed. The as-prepared nanostructures showed a very high specific surface area and demonstrated an excellent ability to remove organic pollutants from wastewater which was manifested in its uptake of various dyes like RhB and MB in aqueous solution within a few minutes. The adsorption efficiency of our $MnWO_4$/$MnMoO_4$ nanostructures were much higher than those of previously reported transition metal oxide nanostructures including Mn_3O_4, Fe_2O_3, MnO_2 as well as other alternative adsorbents such as MCM-22, fly ash, and red mud where the minimum time taken for adsorption was typically more than an hour. $MnWO_4$ also proved to be a good sorbent for Cu(II) ions. The sorption of Cu(II) ions is around 75 and 89.8 % for the molybdate and tungstate sorbents respectively. Kinetic modeling of Cu(II) adsorption showed that the process followed a pseudo first order model. These studies showed that there is a possible application for the complete and fast removal of the organic dyes in presence of inorganic cations using $MnWO_4$/$MnMoO_4$ sorbents. The binding of these dyes with tungstate surface mainly involves physisorption whereas that on molybdate surface is primarily mild chemisorption as analyzed from the UV-vis absorption and FT-IR spectra. Moreover, the adsorbed dyes could be desorbed from the nanosorbent surface by annealing at 225°C and they showed significant multicyclic adsorption efficiency.

References

1. M. T. Uddin, M. A. Islam, S. Mahmud and M. Rukanuzzaman, *J. Hazard. Mater.,* 2009, **164**, 53-60.
2. C. A. Murray and S. A. Parsons, *Water Sci. Technol.: Water Supply,* 2004, **4**, 113-119.
3. E. Forgacs, T. Cserhati and G. Oros, *Environ. Int.,* 2004, **30**, 953-971.
4. R.S. Juang and H.J. Shao, *Adsorption*, 2002, **8**, 71-78.
5. W.S.W. Ngah, A. Kamari and Y.J. Koay, *Int. J. Biol. Macromol*., 2004, **34**, 155-161.
6. S. A. Parsons and B. Jefferson*, Introduction to Potable Water Treatment Processes*; Blackwell Publishing: Oxford, United Kingdom, 2006.
7. H. Y. Shu, C. R. Huang and M. C. Chang, *Chemosphere,* 1994, **29**, 2597-2607.
8. C. All_egre, P. Moulin, M. Maisseu and F. Charbit, *J. Membrane Sci*., 2006, **269**, 15-34.
9. U. Pagga and K. Taeger, *Water Res*., 1994, **28**, 1051-1057.
10. K. Santhy and P. Selvapathy, *Bioresour. Technol*., 2006, **97**, 1329-1336.
11. R. Han, D. Ding, Y. Xu, W. Zou, Y. Wang, Y. Li and L. Zou, *Bioresour. Technol*., 2008, **99**, 2938-2946.
12. J. Geng, J.J. Zhu, D.J. Lu and H.Y. Chen, *Inorg. Chem*., 2006, **45**, 8403-8407.
13. D. Chen, G.Z. Shen, K.B. Tang, Z.H. Liang and H.G. Zheng, *J. Phys. Chem., B* 2004, **108**, 11280-11284.
14. H.T. Shi, X.H. Wang, N.N. Zhan, L.M. Qi and J.M. Ma, *J. Phys. Chem. B,* 2006, **110**, 748-753.
15. B. Moreno, E. Chinarro, M.T. Colomer and J.R. Jurado, *J. Phys. Chem. C*, 2010, **114**, 4251-4257.
16. Y. Ping, Y. Guang-Qing and L. Jian- Nua, *Inorg. Chem. Comm.,* 2004, **7**, 389-391.
17. W. Qu, W. Wlodarski and J. U. Meyer, *Sens. Actuators, B*, 2000, **64**, 76-82.
18. A. H. Arkenbout, T. T. M. Palstra, T. Siegrist and T. Kimura, *Phys. Rev. B: Condens. Matter Mater. Phys.*, 2006, **74**, 184431.
19. O. Heyer, N. Hollmann, I. Klassen, S. Jodlauk, L. Bohaty, P. Becker, J. A. Mydosh, T. Lorenz and D. Khomskii, *J. Phys.: Condens. Matter*, 2006, **18**, L471.
20. K. Taniguchi, N. Abe, T. Takenobu, Y. Iwasa and T. Arima, *Phys. Rev. Lett.,* 2006, **97**, 097203.
21. Y. Xing, S. Song, J. Feng, Y. Lei, M. Li and H. Zhang, *Solid State Sci.,* 2008, **10**, 1299-1304.
22. L. Zhang, C. Lu, Y. Wang and Y. Cheng, *Mater. Chem. Phys.,* 2007, **103**, 433-436.
23. S. Lei, K. Tang, Z. Fang, Y. Huang and H. Zheng, *Nanotechnology*, 2005, **16**, 2407-2411.
24. H.Y. He, J.F. Huang, L.Y. Cao and J.P. Wu, *Desalination,* 2010, **252**, 66-70.
25. Y. Mi, Z. Huang, Z. Zhou, H. Feilong and Q. Meng, *J. Phys. Confer. Series,* 2009, **188**, 012056.
26. J. Maier, *Solid State Ionics*, 2004, **175**, 7-12.
27. S. M. Montemayor and A. F. Fuentes, *Ceram. Int.,* 2004, **30**, 393-400.
28. M. Jang, T.J.R. Weakley and K.M. Doxsee, *Chem. Mater.,* 2001, **13**, 519-525.
29. Thanh-D. Nguyen, D. Mrabet, Thi-Thuy-D. Vu, Cao-T. Dinh and Trong-O. Do, *Cryst. Eng. Comm.,* 2011, **13**, 1450–1460.
30. A. K. Chakraborty, S. Ganguli and M. A. Kebede, *J. Clust. Sci.,* 2012, **23**, 437–448.
31. C. Sekar, R. Kalai Selvan, S.T. Senthilkumar, B. Senthilkumar and C. Sanjeeviraja, *Powder Tech.,* 2012, **215-216**, 98–103.

32. P. V. Hanh, L. H. Hoang, P. V. Hai, N. V. Minh, Xiang-B. Chen and In-S. Yang, *J. Phys. Chem. Sol.,* 2013, **74**, 426–430.
33. M. H. Fulekar, A. Singh, D. P. Dutta, M. Roy, A. Ballal and A. K. Tyagi, *RSC Advances*, 2014, **4**, 10097 – 10107.
34. A. Singh, D. P. Dutta, M. Roy, A. K. Tyagi and M. H. Fulekar, *J. Mater. Science,* 2014, **49**, 2085-2097.
35. Y.S. Ho, C.T. Huang and H.W. Huang, *Process Biochem.* 2002, **37**, 1421-1430.
36. B. Ingham, S.V. Chong and J. L.Tallon, *Curr. Appl. Phys.* 2006, **6**, 553-556.
37. S. Brunauer, P.H. Emmett and E. Teller, *J. Am. Chem. Soc.* 1938, **60**, 309-319.
38. Z. Zhang and J. Kong, *J. Hazard. Mater.* 2011, **193**, 325– 329.
39. B. Saha, S. Das, J. Saikia and G. Das, *J. Phys. Chem. C* 2011, **115**, 8024–8033.
40. B.H. Hameed, A.L. Ahmad and K.N.A. Latiff, *Dyes and Pigments,* 2007, **75**, 143-149.
41. R. Chen, J. Yu and W. Xiao, *J. Mater. Chem. A*, 2013, **1**, 11682–11690.
42. S. Wang, H. Li, L. Xu, *J. Colloid Interface Sci.*, 2006, **295**, 71-78.
43. V. K. Gupta, D. Mohan, S. Sharma, M. Sharma, *Sep. Sci. Technol*., 2000, **35**, 2097-2113.
44. S. Wang, Y. Boyjoo, A. Choueib, Z. H. Zhu, *Water Res.,* 2005, **39**,129-138.
45. J. Fei, Y. Cui, X. Yan, W. Qi, Y. Yang, K. Wang, Q. He, J. Li, *Adv. Mater.*, 2008, **20**, 452-454.
46. R.W. Gaikwad, S. A. Misal, *Int. J. Chem. Engg. Appl*., 2010, **1**, 342-345.
47. Y. E. Mouzdahir , A. Elmchaouri , R. Mahboub , A. Gil , S.A. Korili, *Desalination*, 2010, **250**, 335-338
48. Y. S. Ho and G. McKay, *Process Saf. Environ. Prot.,* 1998, **76B**, 183-191.
49. Y. S. Ho and G. McKay, *Water Res.*, 2000, **34**, 735-742.
50. P. Tarte and M. Liegeois-Duyckaerts*, Spectrochim. Acta—Part A,* 1972, **28A**, 2029-2036.
51. S. Lei, K. Tang, Q. Liu, Z. Fang, Q. Yang, H. Zheng, *J. Mater. Sci.,* 2006, **41**, 4737-4743.
52. T.S. Sian and G.B. Reddy, *Appl. Surf. Sci.,* 2004, **236**, 1–5.
53. K.M. Garadkar, L.A. Ghule, K.B. Sapnar and S.D. Dhole, *Mater. Res. Bull.,* 2013, **48**, 1105–1109.